CrossMark

Effect of electron beam irradiation on the microstructure, optical and electrical properties of glass resistive plate chamber detector material

K. V. Aneeshkumar[1] · S. Krishnaveni[1] · C. Ranganathaiah[2] · H. B. Ravikumar[1]

Abstract The glass resistive plate chamber (RPC) detector materials were exposed to 8 MeV electron beam from 20 to 100 kGy in steps of 20 kGy. In order to study the electron beam irradiation-induced effects in glass RPC detector material, positron annihilation lifetime spectroscopy (PALS), X-ray diffraction (XRD) and Fourier transform infrared (FTIR) spectroscopic investigations were carried out. PALS analysis at lower electron doses indicates the increased void size with the creation of additional sites in the glass network. This is attributed to the breakage of Si–O bonds at the regular tetrahedral sites of Si–O–Si up to 40 kGy. The reduced void size at higher irradiation doses indicates the increased chemical bonding between the tetrahedral sites of Si–O–Si and hence increases the short-range order in the silica glass. These changes are complement with the XRD, FTIR results and the measured electrical conductivity. The variation of AC conductivity with frequency obeys Jonscher power law in all the electron irradiation doses at room temperature. The variation in optical band gap energy from the ultraviolet–visible (UV–Vis) spectra inferred the elimination of defects accumulation at higher irradiation doses due to the glass network close packing.

✉ H. B. Ravikumar
   hbr@physics.uni-mysore.ac.in

1   Department of Studies in Physics, University of Mysore, Manasagangotri, Mysuru 570006, India

2   JSS Technical Institutions, JSSTI Campus, Mysuru 570006, India

1 Introduction

India-based neutrino observatory (INO) [1] is a multi-institutional collaborative project that has proposed to study neutrino oscillations and its associated parameters [2]. The resistive plate chambers (RPCs) [1, 2] are used as the active detectors in this basic science project to explore the mysterious properties of atmospheric neutrinos. The RPC is a gas-filled detector with gas enclosed between the two parallel plates of large bulk resistivity kept at high voltages, which are made up of materials like glass or bakelite. As the RPC detectors are operated at high voltages for longer time, the time resolution and efficiency of the detector get affected due to high leakage current [3, 4].

The clear float glasses with a bulk resistivity in the order of 10^{10}–10^{12} Ωcm, procured from M/s Asahi Float Glass (India) Ltd and M/s Saint-Gobain (India) Ltd are used as the electrode materials for the fabrication of glass RPC detectors in INO project. The previous experimental investigations on these glass samples suggest that Asahi glass is qualitatively better glass compared to other glasses due to its surface smoothness and efficiency [5]. The glass RPCs used in high-energy physics experiments undergoes deterioration under direct mechanical stress, temperature and high-energy radiations. This may be due to the structural alterations in the amorphous glass upon various environmental conditions [6]. Recently, Sarika Bhide et al. [7] reported that the deterioration in the efficiency of the detector is associated with the quality of glass plates used to fabricate the RPC detectors.

The iron calorimeter (ICAL) detector at INO will employ large number of Asahi glass RPCs of about 2 m × 2 m area for the detection of atmospheric neutrinos. In the long run, due to its extensive use in the radiation-rich environment,

there will be some modifications in the microstructure of this silica-based glass detector material. Therefore, it is important to carry out detailed microstructural characterization of Asahi float glasses to test the survivability of the detectors in the radiation-rich environment. Literature survey reveals that the irradiation of high-energy radiations like electrons, gamma rays and UV radiations produces significant changes in the Si–O–Si chemical bonds and hence modifies the desired physical and chemical properties of the silica-based glass structure [8–12].

In the present study, in order to understand the factors responsible for the structural modifications in glass RPC detectors and to improve the performance, we have exposed Asahi glass samples to 8 MeV electron beam with different irradiation doses. The microstructural characterization of electron beam-irradiated Asahi float glass material has been carried out by making use of one of the well-established techniques, viz., positron annihilation lifetime spectroscopy (PALS) [13–15]. Several research groups are working on positron trapping and positronium formation in various types of silica-based glasses [14, 16]. However, the nano-voidal studies and its relationship with the electrical conductivity in Asahi float glass RPC detector materials upon 8 MeV electron beam irradiation have been nowhere reported. Therefore, the present study provides better insight into understanding the irradiation-induced effects on Asahi glass material for the RPC detector fabrication. Other experimental techniques such as XRD, FTIR and UV–Vis spectroscopy are also used to explore the effect of electron beam irradiation on the Asahi glass RPC detector material. In addition, we have attempted to explain the effect of electron beam irradiation on the microstructure and the electrical conductivity of Asahi glass material to achieve a better detector performance for the extended period. Furthermore, the variation of AC conductivity and frequency is also correlated with Jonscher power law.

2 Experimental

2.1 Electron beam irradiation

AIS brand clear float glasses of density 2.5 g cm^{-3} manufactured by M/s Asahi Float Glass (India) Ltd., Mumbai, India, are used in the present investigation. These glasses are used in the fabrication of RPC detectors for INO research project at TIFR Mumbai, India. The chemical composition of the elements present in Asahi (AIS brand clear float) glasses and SGG clear float glass (Planilux) from M/s Saint-Gobain (India) Ltd is given in atomic weight percentages in Table 1 [5]. The rectangular pieces of AIS brand clear float glass samples having dimensions 1 cm × 1 cm and thickness 0.28 cm were

Table 1 Chemical composition of different glass RPC detector materials in atomic weight percentage

Element	Percentage of elements in different float glasses	
	Asahi glass	Saint-Gobain glass
C	4.89	–
Na	6.89	8.22
Mg	1.79	1.85
Al	0.32	0.27
Si	21.73	24.56
Ca	2.71	3.32
O	61.67	59.97
Sn	–	0.58
F	–	1.23

Table 2 Specifications of electron beam irradiation

Beam energy	8 MeV
Pulse repetition rate (PRR)	31 Hz
Average beam current	80 μA
Pulse width	10 μs
Source to surface distance (SSD)	75 cm
Scanning	4.0 A @ 200 ms
Dose rate	2 kGy/pass

exposed to 8 MeV electron beam with an average current 80 μA at Raja Ramanna Centre for Advanced Technology, Indore, Madhya Pradesh, India. The details of electron beam specifications are given in Table 2. The samples were exposed to different doses up to 100 kGy in the interval of 20 kGy and the same were used for PALS, XRD, FTIR, AC, DC conductivity studies and optical measurements.

2.2 Positron annihilation lifetime measurements

Positron annihilation lifetime measurements were carried out for as-received and 8 MeV electron beam-irradiated Asahi glass samples using fast–fast coincidence positron lifetime spectrometer. Consistently reproducible spectra were analyzed into three lifetime components with the help of a computer program PATFIT-88 [17] with proper source and background corrections. The ortho-positronium (o-Ps) lifetime (τ_3) is related to the void size by a simple empirical relation given by Nakanishi et al. [18], initially proposed by Tao [19] for molecular liquids and later by Eldrup et al. [20]. In this model, positronium is assumed to be localized in a spherical potential well having an infinite potential barrier of radius R_o with an electron layer in the region $R < r < R_o$. The relation between 'τ_3' and the radius 'R' of the void size is,

$$\lambda = \frac{1}{\tau_3} = 2P$$
$$= 2\left[1 - \left(\frac{R}{R_0}\right) + \left(\frac{1}{2\pi}\right)\sin\left(\frac{2\pi R}{R_0}\right)\right] \text{ ns}^{-1} \qquad (1)$$

where $R_o = R + \delta R$ and δR is an adjustable parameter and P represents the probability of positronium (Ps) formation at the electron layer thickness δR. By fitting Eq. (1) with τ_3 values for known hole sizes in porous materials like zeolites, a value of $\delta R = 0.166$ nm was obtained [18]. With this value of δR, the void radius 'R' has been calculated from Eq. (1) and the average void size (V_f) is evaluated as $V_f = (4/3) \pi R^3$. The fractional void or the void content (F_v) can also be estimated as $F_v = C\, V_f\, I_3$, where C is structural constant, 0.0018 Å^3, V_f is the void size and I_3 is the o-Ps intensity. The detailed theory and the positron lifetime measurements can be found elsewhere [13, 15].

2.3 XRD, FTIR, UV–Vis and conductivity studies

XRD spectra of as-received and 8 MeV electron beam-irradiated Asahi glass samples at different electron irradiation doses have been recorded using powder X-ray diffractometer RIGAKU-DENKI II miniflex with Ni-filtered CuKα X-rays of wavelength 1.5406 Å. The crystallinity of as-received and electron beam-irradiated glass samples was calculated from the ratio of area under the crystalline peaks to the total area using computer program PeakFit 4.1. FTIR spectra for as-received and electron beam-irradiated glass samples upon different doses were recorded in the wave number range of 4000–600 cm^{-1} using Spectrum Two 94012 Spectrometer with a resolution of 4 cm^{-1}.

The DC electrical conductivity of as-received and 8 MeV electron beam-irradiated glass samples was measured using Keithley 2636A System SourceMeter. AC conductivity measurements were also made using LCR HiTester Hioki (Japan) 3532-50 programmable computer-interfaced digital LCR impedance meter in the frequency range of 100 Hz to 5 MHz at room temperature. The detailed measurements can be found elsewhere [15]. In addition, ultraviolet–visible absorbance and transmittance spectra were also recorded for as-received and electron beam-irradiated Asahi glass samples using Shimadzu UV-1800 spectrometer in the wavelength region of 190–900 nm.

3 Results and discussion

3.1 Positron annihilation lifetime spectroscopy results

The positron annihilation lifetime spectroscopy (PALS) result provides basic information about void size (V_f) and

their concentration in glass samples. As we are interested in void size and their concentration in Asahi glass samples upon electron beam irradiation, only the third and long lifetime component, viz., o-Ps lifetime (τ_3) and o-Ps intensity (I_3) derived from PATFIT-88 program are explicitly explained in this paper. However, along with o-Ps lifetime (τ_3) and intensity (I_3), the variation of second lifetime (τ_2) and its intensity (I_2) is also taken into consideration to explain the structural changes and conductivity in Asahi glass samples upon irradiation which are reported in Table 3.

Figures 1, 2 show the variation of o-Ps lifetime (τ_3), void size (V_f) and o-Ps intensity (I_3), fractional voids (F_v) of 8 MeV electron beam-irradiated Asahi glass samples, respectively. In Fig. 1, about 175 ps increase in o-Ps lifetime (τ_3) is seen from as-received to 40 kGy electron beam-irradiated Asahi glass samples. This is reflected in the increased 14.73 Å^3 void size from 57.62 to 72.35 Å^3 at 40 kGy and then reduced to 55.62 Å^3 at 100 kGy electron beam irradiation dose.

The increased o-Ps lifetime (τ_3) suggests to the increased void size in the silicate glass structure due to the impact of high energetic electron beam. It is well known that electron beam irradiation with small doses easily breaks the ionic bonds between the terminated sodium ions and its chained oxygen in silica network structure. Therefore, the increased void size upon lower irradiation doses attributed to the breakage of Si–O chemical bonds and the reduced void size is due to the increased silica glass network cross-linking upon higher irradiation doses [14, 21]. Mohapatra et al. reported the formation of silicon-based hole centers in silicate glasses after irradiation with electrons due to the breakage of Si–O bonds at the regular tetrahedral sites of Si–O–Si [22]. Therefore, the increased void size in the glass at lower doses attributed to the cleavage of Si–O bonds [22] and the formation of free radicals or free electrons. The relaxation of the molecular stress in silica glassy network originated by the dangling bonds of weakly bonded metal–oxygen pairs [23, 24]. This may initiate the disorders in the original structure of the glass matrix causing the formation of defect centers accompanied with changes in void size.

There is a noticeable decrease of about 200 ps in o-Ps lifetime (τ_3) and 16.73 Å^3 void size (V_f) starting from 40 to 100 kGy electron irradiation doses. The reduced void size after 40 kGy irradiation dose is attributed to the network cross-linking of Si–O–Si bonds in the silicate glass [25]. In general, the structure of glass exhibits high degree of short-range periodicity due to the chemical bonding between the Si–O–Si tetrahedral and forms many polyhedral structures [26]. The increased chemical bonding at the tetrahedral sites of the glass network increases the polyhedral structure at higher irradiation doses and hence reduces the void size

Table 3 Positron lifetime results of as-received and electron beam-irradiated Asahi glass samples at different doses

Dose (kGy)	τ_2 (ns)	τ_3 (ns)	I_2 (%)	I_3 (%)	V_f (Å^3)
0	0.382 ± 0.003	1.546 ± 0.017	63.08 ± 0.43	15.47 ± 0.25	57.62 ± 1.03
20	0.394 ± 0.003	1.686 ± 0.015	63.55 ± 0.43	15.09 ± 0.21	69.29 ± 1.07
40	0.398 ± 0.003	1.721 ± 0.014	63.67 ± 0.40	15.19 ± 0.19	72.35 ± 1.05
60	0.389 ± 0.003	1.689 ± 0.016	66.44 ± 0.44	15.36 ± 0.22	69.54 ± 1.14
80	0.383 ± 0.003	1.603 ± 0.016	66.43 ± 0.46	16.03 ± 0.25	62.36 ± 1.10
100	0.374 ± 0.003	1.521 ± 0.018	64.98 ± 0.48	16.57 ± 0.28	55.62 ± 1.13
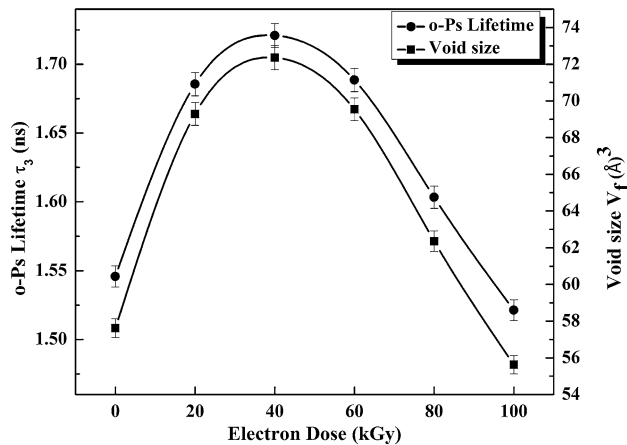
Fig. 1 Variation of o-Ps lifetime (τ_3) and void size (V_f) as a function of electron dose
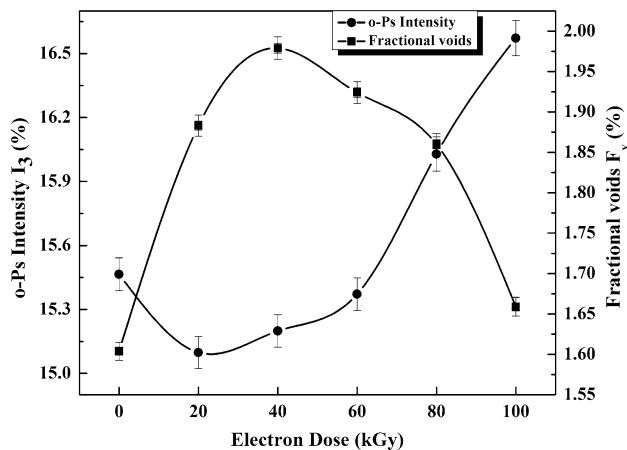
Fig. 2 Variation of o-Ps intensity (I_3) and fractional voids (F_v) as a function of electron dose

in the glass network. The possibility of shrinkage of O–Si–O molecules and the close packing of tetrahedral network cannot be ruled out [27, 28]. This close packing in the glass network hinders the glassy chain mobility and enhances the rigidity of the glass structure [23, 29].

It is important to note that the second lifetime (τ_2), which is assigned to the annihilation of trapped positrons, is also exhibiting almost similar behavior as o-Ps lifetime (τ_3) does. The intensity I_2 exhibits around 3.36% increase

from 63.08 to 66.44% to the irradiation dose of 60 kGy. The increase in I_2 is due to the oxygen enrichment of the trapping sites and annihilation of positrons at negative charged oxygen-related defects as evidenced by the decrease in lifetime τ_2 at higher irradiation doses [16].

In addition to the major elements like C, Na, Mg, Al, Si and O, large amount of alkali impurities Na_2O, CaO and MgO were also present in the Asahi float glass material [5]. Na^+, Ca^{2+} and Mg^{2+} cations act as the network modifiers and perturb the continuity of the glassy network due to the cleavage of Si–O–Si bonds leading to the formation of non-bridging oxygen groups (Si–O–NBO) [30]. This may also alter the void size upon electron irradiation doses in Asahi float glass material.

In Fig. 2, it is observed that there appears to be the slight decrease in o-Ps intensity (I_3) at 20 kGy and increases to 16.57% at 100 kGy irradiation dose. The increased o-Ps intensity (I_3) at 100 kGy is probably due to the creation of more number of voids upon higher electron irradiation doses. The variation of fractional void (F_v) as a function of electron irradiation dose is also reported in Fig. 2. There is about 0.4% of increase in fractional void (F_v) from as-received glass samples to 40 kGy electron beam irradiation doses. There is a slight decrease in fractional void (F_v) after 40 kGy irradiation doses owing to the overall reduction in void. This is also due to the close packing of silica glass tetrahedral network upon higher electron irradiation doses.

3.2 XRD results

The amorphous nature of XRD spectra of as-received and 8 MeV electron beam-irradiated Asahi glass samples is shown in Fig. 3. The electron beam irradiation modifies the microstructure of Asahi glass RPC detector materials, clearly revealed by the observed remarkable changes in the XRD spectra. As we can see from the XRD spectra, as-received Asahi glass does not show any crystalline peak. However, the electron beam-irradiated Asahi glass samples having 20–80 kGy in the interval of 20 kGy doses exhibit an extra prominent X-ray peak at about 17° and 22°. The prominent peaks observed at 40 and 60 kGy of irradiation doses exhibit reduced FWHM compared to other electron
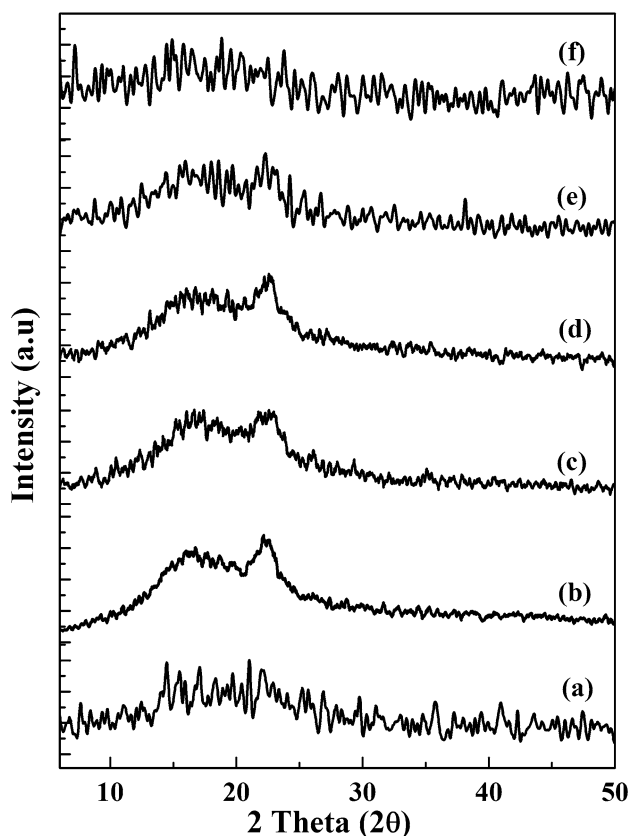
Fig. 3 XRD spectra of as-received and electron beam-irradiated Asahi glass samples [(a–f) represents the XRD spectra of as-received to 100 kGy electron beam-irradiated samples in the interval of 20 kGy, respectively]
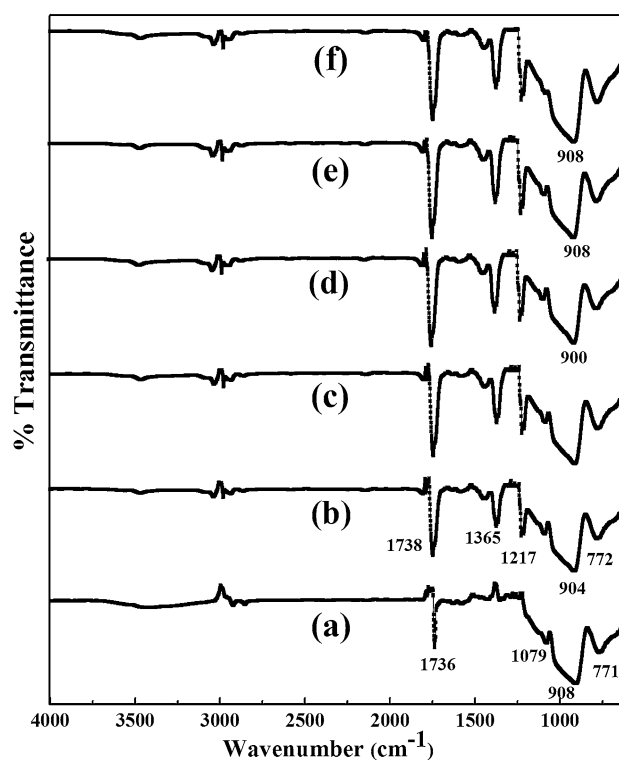

Fig. 4 FTIR spectra of as-received and electron beam-irradiated Asahi glass samples [(a–f) represents the FTIR spectra of as-received to 100 kGy electron beam-irradiated samples in the interval of 20 kGy, respectively]

irradiation doses. This can be attributed to the initialization of close packing and the reduced bond length of silica chains of the glass network, which slightly increases the crystallinity of Asahi glass samples due to the energetic electron beam.

The calculated crystallinity value of as-received Asahi glass RPC detector material in the present study is around 12.26%, which is almost equal to the crystallinity value of highly amorphous glass samples reported in the literature [31]. The clear peak at 60 kGy irradiated sample shows about 14.72% of crystallinity due to the increased close packing network of glass structure. The significant increase in intensity of the major peak at 60 kGy electron dose is due to the enhancement in the percentage of crystallinity. Therefore, the increased percentage of crystallinity upon higher irradiation dose is attributed to the increased chemical bonding between the tetrahedral sites and increased short-range order in the silica glass due to its network close packing [25–27]. The slight reduction in crystallinity above 60 kGy is due to the vibrations of Si–O–Si bonds in the silica glass structure with the impact of high-dose electron irradiation.

3.3 FTIR results

The Fourier transform infrared spectroscopy is a significant method used for understanding variations in the functional groups of a variety of materials upon external treatments. In this paper, FTIR is used to monitor the changes in functional group in the Asahi RPC glass structure upon electron beam irradiation which is shown in Fig. 4. In the FTIR spectrum of Asahi glass, the major transmittance bands are at the wave numbers 1736, 1079, 909 and 768 cm^{-1}, respectively. The active vibrations of the silicate groups are expected at the wave number region less than 1500 cm^{-1}. The stretching vibrations of Si–O–Si in SiO$_4$ tetrahedra are usually observed in the wave number range 900–1200 cm^{-1} depending on the cations present in the glass [22]. The transmission band at 1079 cm^{-1} corresponds to the symmetric stretching vibrations of Si–O–Si bridge involving the displacement of the oxygen atom in the tetrahedral network. The observed band in the wave number region 771 cm^{-1} corresponds to the bending mode in the Si–O plane (Si–O stretching) [32, 33].

In electron beam-irradiated sample, the formation of additional bands is observed in the wave number range 1365 and 1217 cm^{-1} at the irradiation dose from 20 to 100 kGy. The sharp bands at 1217 and 1736 cm^{-1}

correspond to the asymmetric stretching of –Si–O–Si– bonds and H-related band in SiO_2, respectively [34, 35]. Therefore, the slight shift in these two bands and the marginal decrease in the percentage of transmittance upon higher doses clearly infer the effect of electron irradiation. The significant peak broadening observed in the wave number region 908 cm^{-1} corresponds to the stretching vibrations of Si–O–Si bonds. This band was shifted to 900 cm^{-1} at 60 kGy electron irradiation maybe due to the breakage of Si–O–Si bonds and at 100 kGy the same band is again shifted to 908 cm^{-1}. However, the band between 900 and 1000 cm^{-1} and 1365 cm^{-1} are also associated with the Si–O bond with one non-bridging oxygen (Si–O–NBO) per SiO_4 tetrahedral structure [22, 30]. The intensity of this transmission band decreases continuously with the increasing electron irradiation doses. These changes in the functional groups suggest the structural modification in the glass network due to breakage of prominent Si–O bonds and the formation of non-bridging oxygen atoms upon electron irradiation [35].

FTIR results also reveal that 8 MeV of electron irradiation will not affect much on the basic functional group of glassy chains and it will not affect the covalent structure and hence the chemical or physical properties of the glass materials predominantly. The rearrangement of the glass network due to the formation of free radicals after the chain breakage and network close packing upon electron beam irradiation contributes much for the microstructural modifications in the glass matrix.

3.4 Electrical conductivity results

3.4.1 Relationship between void size and DC conductivity

The electrical conductivity of silicate glass is basically due to the movement of charge carriers under the influence of external electric field. However, the expansion of glass network, which is related to the available void size, is a key parameter for determining the variations in conductivity. The literature survey reveals that the magnitude of the DC conductivity in glass is mainly depends on the concentration of the charge carriers and their mobility [36]. Figure 5 shows the variation of void size and electrical conductivity as a function of electron dose. The DC conductivity of as-received Asahi glass sample is 5.97×10^{-8} Sm^{-1}. The DC conductivity of electron beam-irradiated glass samples shows maximum values at electron irradiation dose of 20 kGy (5.79×10^{-8} Sm^{-1}). After 20 kGy, DC conductivity decreases and reaches to the minimum value 8.02×10^{-9} Sm^{-1} at the irradiation dose of 100 kGy. The void size (V_f) also exhibits maximum value up to 40 kGy electron irradiation doses. Therefore, the conductivity in Asahi glass at lower doses is the consequence of Si–O–Si
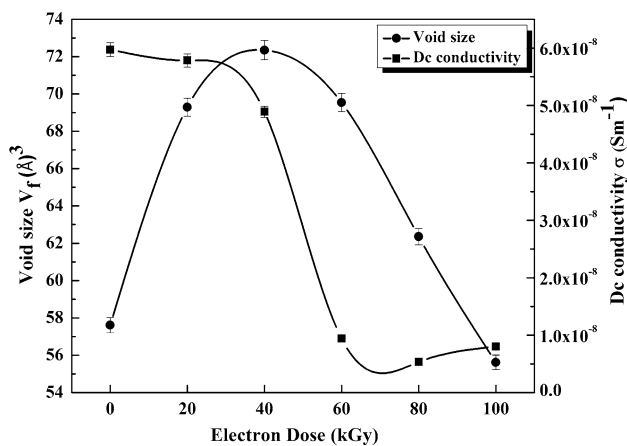

Fig. 5 Variation of void size (V_f) and DC conductivity (σ) as a function of electron dose

bending vibration caused by the displacement of oxygen atom out of the SiO_2 plane and breakage of O–Si–O bonds, which may lead to the formation of electrons and O^{2-} radicals [35, 36]. Therefore, the increased conductivity is probably due to the formation of free charge carriers and increased charge mobility owing to the chain relaxation in the glass matrix.

Generally, alkali ions present in the silicate glasses are known to be the exclusive charge carriers responsible for the electrical properties. Therefore, the reported metallic elements (C, Na, Mg, Al, Si and O) and alkali impurities (Na_2O, CaO and MgO) [5] may influence the generation of more number of charge carriers and hence the DC conductivity. The marginal reduction in electrical conductivity is exhibited after 40 kGy electron irradiation dose. This is in accordance with the reduced void size observed in PALS result at higher irradiation doses. As the network close packing of Si–O–Si bonds are predominant after 40 kGy, the reduced void space restricts the movement of electrons and hence hinders the electrical conductivity.

Both the intensity of positrons annihilating at the trapping sites (I_2) and DC conductivity exhibits higher values below 40 kGy of electron doses. The increased I_2 values due to the oxygen enrichment of the trapping sites lead to an increase in charge carriers mobility and hence the electrical conductivity [37]. The conductivity is exhibiting marginal decrease at higher irradiation doses, maybe due to the reduced number of trapping sites by the Si–O–Si polyhedral network. This is indicated by the reduced I_2 value about 1.46% at 100 kGy electron irradiation dose.

3.4.2 AC conductivity

The dependence of AC conductivity upon electron beam irradiation on different doses with frequency is shown in Fig. 6. It was observed that the AC conductivity increases
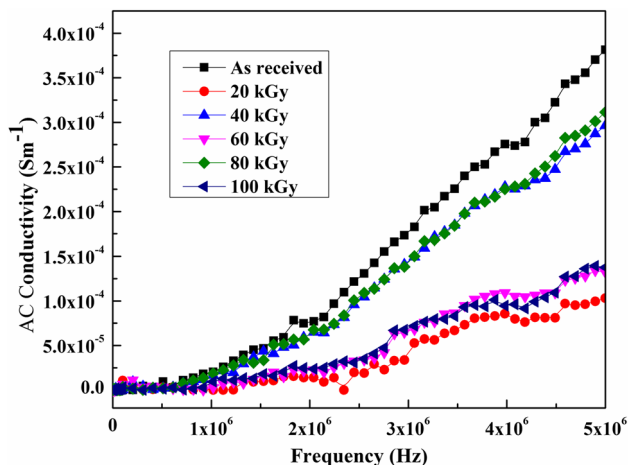
Fig. 6 Variation of AC conductivity as a function of frequency upon different electron doses

continuously from 100 Hz to 5 MHz in all the electron irradiation doses. However, the conductivity of electron beam-irradiated samples at all the irradiation doses is less compared to as-received sample. The increased AC conductivity with frequency may be due to the cleavage of O–Si–O dangling bonds, which may create energetic free electrons, ions and free radicals [23, 30]. Therefore, the increased void size inside the glass provides pathways for the motion of free charge carriers and facilitates the free motion of the electric dipoles. This will allow the charge carriers to hop easily from conducting regions to the neighbors [38] and hence dominates AC conductivity at higher frequencies. This may be the reason for the higher conductivity of the electron beam-irradiated glass samples at 40 kGy. At high frequency, the increase in conductivity is due to the electronic polarization and hopping due to the fluctuation of space charge across the interface causing the intrinsic conduction [39].

In most of the AC conductivity experiments, the conductivity is measured as a function of frequency ω, where $\omega = 2\pi f$ is the angular frequency and 'f' is the linear frequency of an alternating electric field. The relation between frequency and AC conductivity $\sigma_{ac}(\omega)$ has been observed in many amorphous materials and insulators, which has the empirical form: $\sigma_{ac}(\omega) \propto \omega^S$. This relation can be expressed as $\sigma_{ac}(\omega) = A\omega^S$, where A is a constant and S is the frequency exponent. The frequency exponent 'S' is essential in explaining the microscopic origin of the conductivity relaxation in disordered amorphous glass materials after electron beam irradiation.

The AC conductivity variations with frequency obey Jonscher power law [40] in all the doses upon 8 MeV of electron beam irradiation at room temperature. In general, at high frequency and low temperature, the frequency exponent 'S' lies between $0.5 < S < 1$ [41]. The frequency
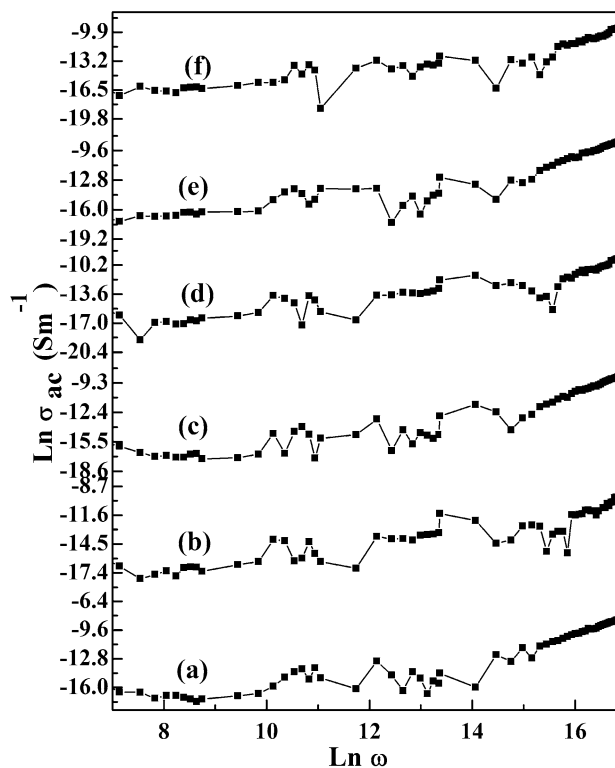

Fig. 7 Variation of Ln $\sigma_{ac}(\omega)$ as a function of Ln ω at different electron doses [(a–f) represents as-received to 100 kGy electron beam-irradiated glass samples in the interval of 20 kGy, respectively]

exponent 'S' were calculated for as-received and electron beam-irradiated Asahi glass samples from the slopes of the straight lines of ln $\sigma_{ac}(\omega)$ verses ln ω, which is shown in Fig. 7. In the present study, the experimentally measured values of 'S' lie between 0.76 and 0.96 for as-received and the electron beam-irradiated glass samples.

3.5 UV–Vis spectroscopy results

The effect of electron beam irradiation on Asahi glass samples through the optical absorption spectra was studied and is shown in Fig. 8. As-received Asahi glass samples exhibit around 90% transmittance for light of wavelengths above 350 nm but the electron beam-irradiated samples show lower transmittance compared to as-received samples. The color of the glass samples changes after electron beam irradiation and become more brownish with the increased irradiation doses. The prominent coloration of the glass sample is attributed to the formation of chromophores due to the electron irradiation-induced bond breakage and reconstruction of close packing of the glass network [28, 42]. This is clearly indicated by the UV–visible spectra, and the main absorption edge shifts gradually toward the longer wavelength from 350 to 362 nm at higher irradiation doses. The shift in absorption edge is
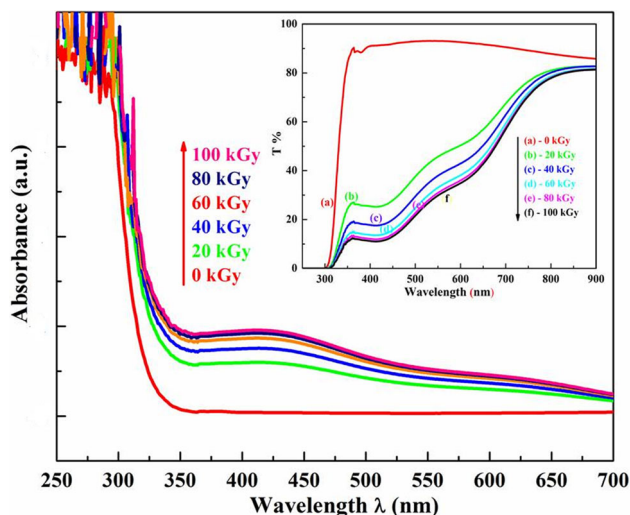
Fig. 8 UV–Vis absorption spectra of as-received and electron beam-irradiated Asahi glass samples (*Inset* UV–Vis transmittance spectra)
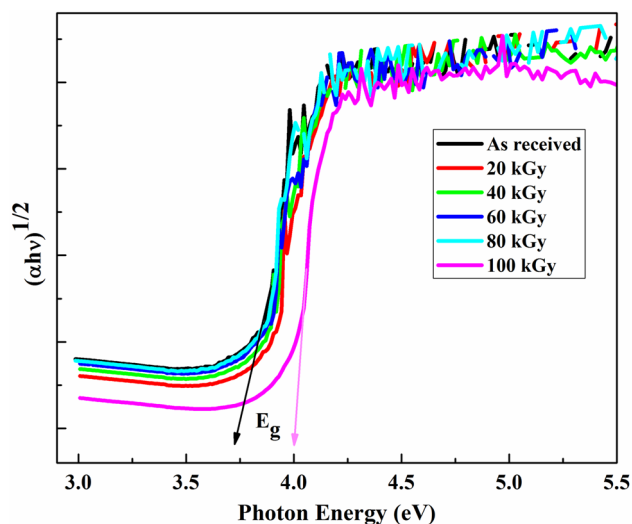

Fig. 9 Variation of $(\alpha h v)^{1/2}$ as a function on photon energy

attributed to the structural disturbance, which may affect the ability of atoms to transmit the light and hence the color and refractive index of the glasses [28].

The optical energy band gap is calculated by translating the observed UV–visible spectra into Tauc's plot (Fig. 9) using the frequency-dependent absorption coefficient $\alpha(v)$ given by Mott and Davis, $\alpha(v) \, h v = B \, (h v - E_g)^r$ [43], where α $(v) = 2.303 A/d$ (A is the absorbance and d is the film thickness), h is Planck's constant, v is the frequency of the incident photons, B is a constant, E_g is the optical energy band gap and $r = 2$ is an empirical index, valid for indirect allowed transitions. A plot of $(\alpha h v)^{1/2}$ Vs $h v$ shows a linear behavior, which can be considered as an evidence for indirect allowed transition. Extrapolation of this linear portion of the curve to zero absorption gives the optical band gap energy E_g. The optical

band gap energy of the RPC glass samples varies with electron doses (3.7–4.0 eV) due to the structural modifications in the form of bond breaking and filling up of the interior voids with the electron. The dominant changes are taking place below 20 kGy irradiation dose is due to the breakage of Si–O bonds in the glass network. It is also clear from Fig. 9 that the band gap energy is around 3.75 eV for 20 kGy irradiated glass samples. This may be the reason for slight reduction in conductivity at 20 kGy electron dose. However, 40–100 kGy electron beam-irradiated glass samples exhibit higher band gap energy between 3.75 and 4 eV. The increased band gap energy reduces the conductivity, which is also supported by the reduced size of voids at the higher irradiation doses. At higher irradiation doses, band gap energy shows greater values compared to the lower doses due to the network cross-linking of Si–O bonds and close packing. In addition to this, there is also a possibility of strain mismatch by the elimination of defects accumulation at higher irradiation doses due to the close packing of Si–O bonds upon electron beam irradiation.

4 Conclusions

The breakage of Si–O bonds at the regular tetrahedral sites of Si–O–Si is the predominant processes under 8 MeV electron beam irradiation of Asahi glass RPC detector material at lower irradiation doses. The increased network close packing between Si–O bonds at higher electron doses possibly enhances chemical bonding between the Si–O–Si chains. The increased chemical bonding between the tetrahedral sites to form polyhedral structure and hence the short-range order in the glass network. This is supported by the reduced void size in the glass network upon higher irradiation doses. The FTIR results suggest that overall Asahi glass network remains unaffected by the electron irradiation. The increased crystallinity at the higher irradiation doses indicate the strengthening of the glass matrix upon electron beam irradiation. The increased band gap energy obtained from the UV–Vis spectra suggests the reduced charge carrier conduction upon higher electron beam irradiation doses. We propose that appropriate electron beam energy and irradiation dose will improve the performance and efficiency of glass RPC detector. Further experimental investigations on these aspects are very essential to get a better understanding of RPC detector performances, and the studies on these lines are in progress.

References

1. M.R. Bhuyan, S.D. Kalmani, N.K. Mondal, S. Pal, D. Samuel, B. Satyanarayana, R.R. Shinde, Nucl. Instrum. Methods A **736**, 135 (2014)
2. N.K. Mondal, Pramana J. Phys. **79**, 1003 (2012)
3. M. Abbrescia, A. Colaleo, G. Iaselli, F. Loddo, M. Maggi, B. Marangelli, S. Natali, S. Nuzzo, Nucl. Instrum. Methods A **515**, 342 (2003)
4. M. Ambrosio, A. Candela, M. De Deo, M.D. Incecco, D. Gamba, A. Giuliano, C. Gustavino, M. Lindozzi, S. Morganti, N. Redaelli, A. Tonazzo, R. Trapani, G.C. Trinchero, Nucl. Sci. Symp. Conf. Rec. IEEE **1**, 605 (2002)
5. D. Kaur, A. Kumar, A. Gaur, P. Kumar, Md Hasbuddin, S. Mishra, P. Kumar, Md Naimuddin, Nucl. Instrum. Methods A **774**, 74 (2015)
6. S.S. Bhide, V.M. Datar, S.D. Kalmani, N.K. Mondal, L.M. Pant, B. Satyanarayana, R.R. Shinde, Nucl. Phys. B (Proc. Suppl.) **158**, 195 (2006)
7. S. Bhide, V.M. Datar, S. Jena, S.D. Kalmani, N.K.M. Mondal, G.K. Padmashree, B. Satyanarayana, R.R. Shinde, P. Verma, Pramana J. Phys. **69**, 1015 (2007)
8. M.A. Marzouk, F.H. Eibatal, Appl. Phys. A **115**, 903 (2014)
9. N. Baydogan, A.B. Tugrul, Solid State Sci. **14**, 1692 (2012)
10. O.A. Podsvirov, A.I. Sidorov, D.V. Churaev, Tech. Phys. **59**, 1674 (2014)
11. N. Jiang, B. Wu, J. Qiu, J.C.H. Spence, Appl. Phys. Lett. **90**, 161909 (2007)
12. A.I. Ignatiev, A.V. Naschekin, V.M. Nevedomsky, O.A. Podsvirov, A.P. Soloviev, A.I. Sidorov, O.A. Usov, Tech. Phys. **56**, 662 (2011)
13. K.V. Aneesh Kumar, H.B. Ravikumar, S. Ganesh, C. Ranganathaiah, IEEE T. Nucl. Sci. **62**, 306 (2015)
14. Y. Sasaki, Y. Nagai, H. Ohkubo, K. Inoue, Z. Tang, M. Hasegawa, Radiat. Phys. Chem. **68**, 569 (2003)
15. K.V. Aneesh Kumar, G.N. Kumaraswamy, C. Ranganathaiah, H.B. Ravikumar, J. Appl. Polym. Sci. **134**, 44962 (2017)
16. R.S. Brusa, S. Mariazzi, L. Ravelli, P. Mazzoldi, G. Mattei, W. Egger, C. Hugenschmidt, B. Löwe, P. Pikart, C. Macchi, A. Somoz, Nucl. Instrum. Methods B **268**, 3186 (2010)
17. P. Kirkegaard, N.J. Pedersen, M. Eldrup, *PATFIT-88: A Data Processing system for Positron Annihilation Spectra on Mainframe and personal Computers*. Denmark Nat. Lab. Reports, RISO-M-**2740** (1989)
18. H. Nakanishi, S.J. Wang, Y.C. Jean, *Positron annihilation in fluids*, in Sharma SC. Singapore: World Scientific **14**, 292 (1988)
19. S.J. Tao, J. Chem. Phys. **56**, 5499 (1972)
20. M. Eldrup, D. Lightbody, Sherwood. Chem. Phys. **63**, 51 (1981)
21. B. Svecova, P. Nekvindova, A. Mackova, P. Malinsky, A. Kolitsch, V. Machovic, S. Stara, M. Mika, J. Spirkova, J. Non-Cryst. Solids **356**, 2468 (2010)
22. M. Mohapatra, R.M. Kadam, R.K. Mishra, D. Dutta, P.K. Pujari, C.P. Kaushik, R.J. Kshirsagar, B.S. Tomar, S.V. Godbole, Nucl. Instrum. Methods B **269**, 2057 (2011)
23. Y. Nishi, A. Kadowaki, T. Shinoda, Mate. Trans. **45**, 3314 (2004)
24. C. Ewing, W.J. Weber, F.W. Clinard, Prog. Nucl. Energy **29**, 63 (1995)
25. A. Tilocca, Proc. R. Soc. A **465**, 1003 (2009)
26. A.K. Yadav, P. Singh, RSC Adv. **5**, 67583 (2015)
27. L.J. Steinbock, J.F. Steinbock, A. Radenovic, Nano Lett. **13**, 1717 (2013)
28. S.L. Srinivasa Rao, G. Ramadevudu, Md Shareefuddin, A. Hameed, M.N. Chary, M.L. Rao, Inter. J. Eng. Sci. Tech. **4**, 25 (2012)
29. Y. Nishi, K. Iwata, Mater. Trans. **47**, 1810 (2006)
30. J. Serra, P. Gonzalez, S. Liste, S. Chiussi, B. Leon, M. Perez-Amor, H.O. Ylanen, M. Hupa, J. Mater. Sci. Mater. Med. **13**, 1221 (2002)
31. G. Brauer, G. Boden, A. Balogh, A. Andreeff, Appl. Phys. **16**, 231 (1978)
32. R. Kitamura, L. Pilon, M. Jonasz, Appl. Optics **46**, 8118 (2007)
33. S. Dreer, P. Wilhartitz, Pure Appl. Chem. **76**, 1161 (2004)
34. B.J. Saikia, G. Parthasarathy, J. Mod. Phys. **1**, 206 (2010)
35. Sh El-Desouki, E.E. Shaisha, A.A. Bahgat, Bulg. J. Phys. **30**, 141 (2003)
36. M.L. Braunger, C.A. Escanhoela Jr., I. Fier, L. Walmsley, E.C. Ziemath, J NonCryst Solids **358**, 2855 (2012)
37. M.H. Abd-El Salam, S. El-Gamal, D.M. Abd El-Maqsoud, M. Mohsen, Arab J. Nucl. Sci. Appl. **46**, 186 (2013)
38. M.G. Veena, N.M. Renukappa, D. Meghala, C. Ranganathaiah, J.S. Rajan, IEEE. T. Dielect. El. In. **21**, 1166 (2014)
39. R.M. Al-Haddad, I.M. Ali, I.M. Ibrahim, I.M. Al-Essa, J. Al-Nahrain Univ **12**, 72 (2009)
40. A.K. Jonscher, Nature **267**, 673 (1977)
41. M. Dult, R.S. Kundu, S. Murugavel, R. Punia, N. Kishore, Physica B **452**, 102 (2014)
42. W. Meulebroeck, K. Baert, H. Wouters, P. Cosyns, A. Ceglia, S. Cagno, K. Janssensd, K. Nys, H. Terryn, H. Thienpont, Proc. SPIE **7726**, 77260D (2010)
43. M.Y. Nadeem, T.B. Sadhana, M. Altaf, M.A. Chaudhry, J. Res. Sci. **5**, 245 (2004)